Catena 185 (2020) 104258

Contents lists available at ScienceDirect

Catena

journal homepage: www.elsevier.com/locate/catena

# Spatial variability of iron oxides in soils from Brazilian sandstone and basalt

Laércio Santos Silva[a,*], José Marques Júnior[a], Vidal Barrón[b], Romário Pimenta Gomes[a], Daniel De Bortoli Teixeira[c], Diego Silva Siqueira[a], Vinícius Vasconcelos[d]

[a] Department of Soils and Fertilizers, Research Group CSME - Soil Characterization for Specific Management, Faculty of Agrarian and Veterinary Sciences, São Paulo State University (FCAV/UNESP), Jaboticabal, São Paulo, Brazil
[b] Department of Agronomy, Córdoba University, Córdoba, Spain
[c] Center of Agrarian Sciences, University of Marília (Unimar), São Paulo, Brazil
[d] Department of Geography, University of Brasília (UnB), Brasília, Distrito Federal, Brazil

ARTICLE INFO

*Keywords:*
Diffuse reflectance spectroscopy
Goethite
Hematite
Pedometrics
Mapping

ABSTRACT

Iron oxides as goethite (Gt) and hematite (Hm) are key minerals to better understand the soil–landscape relationships. Soil samples were collected at three stages of landscape dissection from the geological formations of Vale do Rio do Peixe (sandstone) and Serra Geral (basalt) in the Western Paulista Plateau (WPP), Brazil. Both iron oxides were quantified by X-ray diffraction (XRD) and diffuse reflectance spectroscopy (DRS), and the results were subjected to geostatistical analysis in order to assess the usefulness of DRS for characterizing the spatial variability in Gt and Hm. The prevalence and spatial variability of Hm and Gt in the soils were governed by the sandstone/basalt lithological contrast and landscape dissection. Iron oxides in the clay fraction exhibited high spatial variability over a large area and can be robust indicators of geological diversity and landscape dissection in pedoenvironments with low or high contents of iron oxides. Goethite had the highest spatial variability. Based on the spatial pattern of the differences between DRS and XRD estimates, the saturated red color in soil made DRS less useful for quantifying Hm in environments with high iron oxide contents. The maps indicate the sensitivity of XRD and DRS techniques to represent Hm and Gt spatial variability patterns. Gt was more sensitive to landscape dissection while Hm sensitive to lithology. Thus, the DRS technique is efficient in characterizing the spatial variability of these soil oxides in large areas, even considering the complex relations between soil and landscape.

## 1. Introduction

Outdated soil maps conceal important spatial information and are thus of limited use for agricultural and environmental purposes. Also, they can compromise the feasibility of public policies (Embrapa, 2016) and impair competitiveness in agricultural produce on foreign markets. Agricultural progress in this scenario requires developing effective technologies for determining soil attributes with a view to establishing specific management areas based on soil–landscape models at a detailed scale (Siqueira et al., 2015; Teixeira et al., 2018). The Brazilian National Soil Program "PronaSolos" has undertaken the enormous task of mapping the country's territory at a large scale (1:25 000) over the next 30 years (Embrapa, 2016). One plausible alternative would be improving available knowledge about minerals such as iron oxides in soil, which accurately reflect their formation environment and whose spatial variability is governed by relief and parent material (Camargo et al., 2013).

Iron oxides are major diagnostic attributes in the Brazilian Soil Classification System (Embrapa, 2013), which defines and classifies soils at the family level. Goethite (Gt, α-FeOOH) and hematite (Hm, α-$Fe_2O_3$) are two major components of the clay fraction in tropical soils and used as pedoenvironmental indicators on the grounds of their resisting environmental changes altering soil color (Fitzpatrick, 1988; Cornell and Schwertmann, 2003). The fact that iron oxides strongly influence soil physical and chemical properties (Duiker et al., 2003; Cornell and Schwertmann, 2003; Camargo et al., 2013) makes their spatial characterization essential and raises the need for detailed scale maps to reflect covariate attributes accurately. In recent years many studies have also reported the importance of iron oxides in retaining the leaching of potential hazardous elements (Arenas-Lago et al., 2014; Saikia et al., 2014; Martinello et al., 2014). Therefore to investigate the spatial variability of iron oxides will be of great importance for future environmental studies.

However, quantifying iron oxides is expensive and makes mapping

* Corresponding author.
*E-mail address:* Laerciosantos18@gmail.com (L.S. Silva).

https://doi.org/10.1016/j.catena.2019.104258
Received 10 May 2019; Received in revised form 4 September 2019; Accepted 11 September 2019
0341-8162/ © 2019 Elsevier B.V. All rights reserved.

large areas with conventional techniques such as X-ray diffraction (XRD) unfeasible. In fact, mapping large areas of widely ranging lithology, relief, and soil types requires using fast, accurate, environmentally friendly alternative techniques (Dalmora et al., 2016a,b). Several agricultural sensors have been used in recent decades for the rapid determination of soil attributes (Ferrari et al., 2019; Sánchez-Peña et al., 2018). In this respect, the diffuse reflectance spectroscopy (DRS) technique has been deemed as a promising choice for characterizing Fe oxides (Torrent and Barrón, 2002). In fact, DRS is fast, easy to use, inexpensive (especially with large numbers of measurements), and non-destructive; also, it uses minimal amounts of sample (Guerrero et al., 2010). These advantages have promoted its use in Soil Science. Thus, DRS has enabled the simultaneous determination of many organic and inorganic components (Guerrero et al., 2010), and hence the accurate characterization of soil mineralogy. For example, iron oxides can be identified from their absorption bands in the Vis-NIR spectral region (350–2550 nm), which are associated with specific minerals (Torrent and Barrón, 2008).

Soils in the Western Paulista Plateau (Brazil) are originated mainly from sandstone and, to a lesser extent, basalt. As a result, they span wide ranges of contents in iron oxides including Hm and Gt. However, the ability of DRS to detect small amounts of these two oxides in soils is less usual, and so is its accuracy and efficiency in areas of widely variable geology and geomorphology, which could be assessed by comparison with the traditional choice for this purpose, using XRD. However, assessing the usefulness of DRS in this context requires considering the pedoenvironmental specificities (e.g., lithology, relief, grain size distribution, and morphology) of the target area in order to expose any technical limitations and evaluate the potential indication of this technique.

In this study, we assessed the efficiency of DRS for estimating the spatial variability in Gt and Hm in the framework of soil–landscape relationships in the Western Paulista Plateau (Brazil) to facilitate the development of ancillary methods for mapping large areas.

## 2. Material and methods

### 2.1. Site and geomorphological background

The study area was located in the Western Paulista Plateau, which spans about 13 million hectares (roughly 45% of the São Paulo state, Brazil). Also, their locations spanned the climatic spectrum of the area. Based on the classification of Thornthwaite (1948), the climate is tropical with dry winters ($C_2rA'a'$) in the north and northwest; humid temperate with hot summers ($B_4rB_4'a$) in the south; and temperate humid with dry winters and hot summers ($B_2rB_3'a$) in the east and southeast. The natural vegetation consists of Atlantic forest species in the west, and Cerrados in the east and southeast.

Geologically, the Plateau dates from the higher Cretaceous (88–65 million years) and was formed largely (57%) from sandstones in the Vale do Rio do Peixe formation (VRP), Bauru Group, under the basaltic spills (15%) of the Serra Geral formation (SG), and other sedimentary formations (27%) (Fernandes et al., 2007) (Fig. 1a). The landform map was elaborated according to the method proposed by Vasconcelos et al. (2012), based on the geomorphometric signature. The method aims to classify subtle changes in landforms, reducing the subjectivity of identifying compartments by conceptual landscape models (Troeh, 1965; Daniels et al., 1971), applicable at several scales (Teixeira et al., 2018). Information from the Shuttle Radar Topography Mission (SRTM) was used for elaborating the geomorphometric signatures. The SRTM Digital Elevation Model (DEM) is a regular grid with a spatial resolution of 03 arcsec (~90 m) and a vertical accuracy of 15 m (Smith and Sandwell, 2003).

By interpreting the landform intensity map of Fernandes et al. (2007) for the Western Paulista Plateau, Vasconcelos et al. (2012) succeeded in identifying three different levels of landscape dissection, namely: slightly dissected (Sd), moderately dissected (Md), and highly dissected (Hd) (Fig. 1b). The identification of dissection levels was supplemented with field observations intended to confirm the mutual relationships between components of the physical environment. Sd units characterize the most stable landscapes, soft wavy and flat, convex and linear-convex relief, predominating at the top of the landscape, with an altitude of 450–610 m, and occupying an extension of 20,365 ha. Md units dominate the landscape, with an extension of 92,209 ha, found at altitudes of 431–529 m, and soils in evolution processes. Spanning approximately 21,629 ha, Hd units are depressed areas, where drainage networks are located, with the occurrence of less weathered soils and water table fluctuation. It has steep relief, of concave-convex type and V-shaped valleys, whose altitude varies from 250 to 550 m.

### 2.2. Soil sampling

Soil surveys were carried out and six profiles representing the geological diversity and landscape dissection units were selected (Fig. 1(a and, b)) in order to examine the variation of the total iron oxide ($Fe_2O_3$) content with depth as an indicator of lithological contrast. The trenches were dug at altitude from 250 m to the greatest in the Plateau (610 m). The soils are mainly Latosols (Oxisols) or Argisols (Ultisols) (Embrapa, 2013; Soil Survey Staff, 2010).

The state highway map of the Brazilian roads and traffic department was used to construct a sampling plan with the aid of the ET GeoWizards tool in the software ArcView 9.3. A total of 200 samples were collected from the 0.0–0.2 m soil layer at representative points with minimal anthropic interference (Fig. 1a). The shortest and longest distance between sampling points was 10 and 60 km, respectively. The points were well distributed in space to ensure that the samples would be representative of lithology and landscape dissection units (Fig. 1(a and, b)). The number of sampling points used was based on the experience gathered in previous geostatistical studies on WPP (Marques et al., 2015; Teixeira et al., 2018).

### 2.3. Laboratory analyses

#### 2.3.1. Soil

Samples from the studied profiles were analyzed for Si, Al, and Fe by selective dissolution in sulfuric acid. The total contents thus determined were used to calculate $K_i$ and $K_r$ (Embrapa, 2013), which are two measures of soil weathering. Particle size distribution was determined by using a 0.1 M NaOH solution under slow stirring as a dispersant, and the clay fraction was quantified with the pipette method (Embrapa, 2011).

#### 2.3.2. Goethite and hematite

*2.3.2.1. X-ray diffraction.* Clay fraction was used to quantify Gt and Hm by powder XRD. Previously, the oxides were concentrated by boiling in 5 M NaOH, using the method of Norrish and Taylor (1961) as modified by Kämpf and Schwertmann (1982). Measurements were made with a Mini-Flex Rigaku II spectrometer (20 mA, 30 kV) using Cu Kα radiation and a scan rate of 1° 2θ $min^{-1}$. The Hm/(Gt + Hm) ratio was estimated by comparing the areas under the peaks for the two oxides with their proportions in Gt–Hm mixed standards. Mostly, Hm and Gt in the clay fraction were calculated from the difference between the free (Fed) and low-crystallinity iron (Feo) and the Hm/(Gt + Hm) ratio (Kämpf and Schwertmann, 1982). However, for some basaltic soil samples, which also contained maghemite (Mh), we had to deduct the Fe from this phase, which was estimated from the low-frequency magnetic susceptibility measurements, according to Peters and Dekkers (2003). Similar analytical procedure was previously reported by Poggere et al. (2018).

Alternatively, samples were also analyzed by DRS. For this purpose, an amount of 1 g of air-dried fine earth (ADFE) was ground to constant

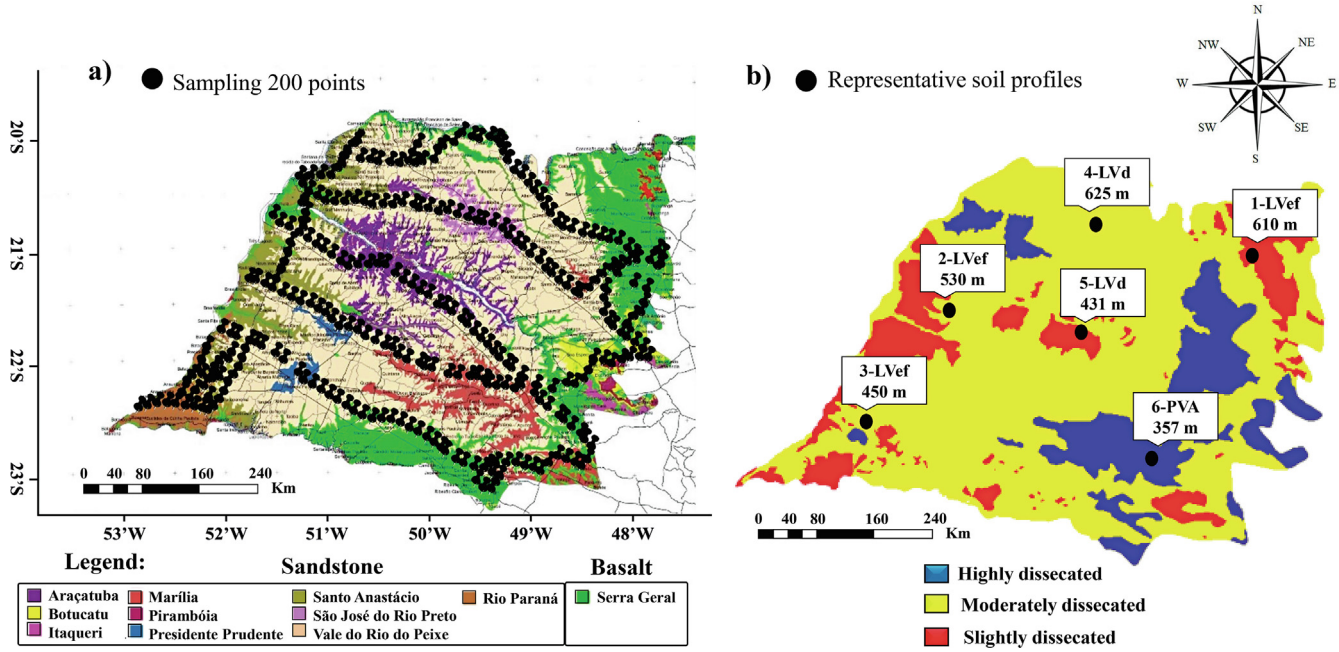


**Fig. 1.** Geological maps (Fernandes et al., 2007) (*a*) and landscape dissection units (Vasconcelos et al., 2012) (*b*) representative soil profiles in the Western Paulista Plateau: 1, 2 and 3 - Rhodic Eutrudox (LVef), 4 and 5 - Rhodic Hapludox (LVd) and 6 - Typic Kandiudalf (PVA) (Soil Survey Staff, 2010).

color in a mortar and placed in a cylindrical holder of 16 mm in diameter. Reflectance measurements ($R$) were obtained with a Lambda 950 UV/Vis/NIR spectrometer coupled to an integrating sphere of 150 mm in diameter. Spectra were recorded at 0.5 nm intervals over the wavelength range of 250–2500 nm (Vis-NIR), using an integration time of 2.43 nm $s^{-1}$ and Halon (PTFE) as a blank.

The spectral data were used to calculate the second derivative of the Kubelka-Munk function over the wavelength range of 380–710 nm (Kubelka and Munk, 1931). A spline procedure involving 30 data points was used to estimate the Hm/(Hm + Gt) ratio according to Scheinost et al. (1998). This procedure allowed comparing DRS potential in the estimation of Gt and Hm obtained by XRD. According to Torrent and Barrón (2002), this procedure allows Gt and Hm contents lower than 0.1% – which is one order of magnitude lower than the limit for the XRD technique – to be determined.

### 2.4. Statistical and geostatistical analyses

The analytical results were initially used to calculate means, maximum and minimum values, medians, standard deviations, coefficients of variation, asymmetry, and kurtosis. The means for landscape dissection units were compared by the Tukey's test (5%), and Gt and Hm contents were estimated from XRD patterns, and the DRS alternative procedure was subjected to regression analysis. XRD and DRS results were compared in terms of the following parameters: coefficient of determination ($R^2$), mean error (ME), standard deviation of the error (SDE), residual prediction deviation (RPD), and root mean square error (RMSE). RPD values were classified according to Chang et al. (2001) as excellent (RPD > 2), acceptable (1.4 < RPD < 2) or unreliable (RPD < 1.4). Usually, accurate models have high $R^2$ and RPD values but low RMSE and SDE values. These parameters were calculated according to Viscarra Rossel et al. (2006).

#### 2.4.1. Spatial variability

Spatial variability of Hm and Gt values obtained with the two techniques was assessed geostatistically. The experimental semivariance was calculated according to Oliver and Webster (2014) criteria from the following equation:

$$\hat{\gamma}(\mathrm{h}) = \frac{1}{2\mathrm{N(h)}} \sum_{\mathrm{i=1}}^{\mathrm{N(h)}} [\mathrm{Z(x_i)} - \mathrm{Z(x_i + h)}]^2 \quad (1)$$

where $\gamma(h)$ is the semivariance at distance $h$, $N(h)$ is the number of pairs used to calculate $h$, $Z(x_i)$ is the value of the attribute $Z$ at position $x_i$, and $Z(x_i + h)$ is the value of the attribute $Z$ at a distance $h$ from $x_i$.

The spherical mathematical model used was fitted to the variograms in terms of the number of pairs used to estimate the semivariance, the sum of the square of residuals (SQR), the presence of a sill in the variograms (Oliver and Webster, 2014), and the coefficient of determination ($R^2$). Once variograms were modeled by $GS^+$ software (Robertson, 1998), the values corresponding to the unknown points were estimated by ordinary kriging and the maps processed with Surfer (1999) software. The degree of spatial dependence (DSD) was estimated from the ratio of the nugget effect ($C_0$) to the sill ($C_0 + C_1$). An attribute was assumed to have high, moderate or low DSD if its $C_0/(C_0 + C_1)$ ratio was lower than 25%, 25–75% or higher than 75%, respectively (Cambardella et al., 1994).

#### 2.4.2. Validation of spectral maps

The spatial patterns for Gt and Hm obtained from XRD and DRS results were compared through traits. The percent variability at a local scale was calculated from the following equation:

$$\Delta(\%) = \frac{\mathrm{DRS} - \mathrm{XRD}}{\mathrm{XRD}} \times 100 \quad (2)$$

A Δ value of up to 20% for XRD values was taken to be acceptable here. This criterion was assumed based on the degree of similarity between DRS and XRD maps and geology (Camargo et al., 2016). Positive and negative Δ values were assumed to represent over- and underestimation, respectively, in an attribute. This parameter allowed us to classify Hm and Gt estimates as acceptable or unacceptable.

## 3. Results and discussion

### 3.1. Physical and chemical properties of soil profiles

The total contents in Fe as $Fe_2O_3$ extracted by sulfuric acid from ADFE ranged from 228 to 14 g $kg^{-1}$ (Table 1). The highest contents

**Table 1**
Oxide contents as determined by sulfuric digestion, sand, silt, and clay contents, weathering indices, and soil color of six typical soils profiles in slightly, moderately, and highly dissected units of SG (basalt) and VRP (sandstone).

| Horizon | Depth | $SiO_2$ | $Al_2O_3$ | $Fe_2O_3$ | Sand | Silt | Clay | | | Munsell color |
|---|---|---|---|---|---|---|---|---|---|---|
| | (m) | (g kg$^{-1}$) | | | (g kg$^{-1}$) | | | $K_i$[1] | $K_r$[2] | |
| 1 - Rhodic Eutrudox (Eutroferric Red Latosol, LVef) from a slightly dissected unit in SG (Soil Survey Staff, 2010) | | | | | | | | | | |
| Ap | 0–0.2 | 130 | 360 | 211 | 120 | 240 | 650 | 0.61 | 0.45 | 2.5YR 3/3.5 |
| $Bw_1$ | 0.2–0.5 | 111 | 390 | 227 | 110 | 260 | 630 | 0.48 | 0.35 | 2.5YR 3/4 |
| $Bw_2$ | 0.5–0.9 | 196 | 380 | 228 | 100 | 260 | 640 | 0.88 | 0.64 | 2.5YR 3/4 |
| Bwc | 0.9–2.5 | 137 | 450 | 228 | 100 | 270 | 630 | 0.52 | 0.39 | 2.5YR 3/4 |
| 2 - Rhodic Eutrudox (Eutroferric Red Latosol, LVef) from a moderately dissected unit in SG (Soil Survey Staff, 2010) | | | | | | | | | | |
| A | 0–0.1 | 172 | 355 | 204 | 200 | 450 | 350 | 0.82 | 0.60 | 2.5YR 3/3 |
| AB | 0.1–0.3 | 149 | 358 | 206 | 130 | 370 | 500 | 0.71 | 0.52 | 2.5YR 3/3.5 |
| Bw | 1.6–2.0 | 163 | 375 | 217 | 160 | 370 | 410 | 0.74 | 0.54 | 2.5YR 3/4 |
| Bwc | 2–2.2 | 182 | 345 | 217 | 190 | 400 | 410 | 0.90 | 0.64 | 2.5YR 3/5 |
| 3 - Rhodic Eutrudox (Eutroferric Red Latosol, LVef) from a highly dissected unit in SG (Soil Survey Staff, 2010) | | | | | | | | | | |
| Ap | 0–0.2 | 242 | 278 | 196 | 440 | 100 | 460 | 1.48 | 1.02 | 2.5YR 3/4 |
| Bw | 0.2–0.5 | 260 | 286 | 200 | 400 | 80 | 520 | 1.55 | 1.07 | 2.5YR 3/4 |
| B/C | 0.5–1.2 | 257 | 260 | 198 | 410 | 70 | 520 | 1.68 | 1.13 | 5YR 4/4 |
| 4 - Rhodic Hapludox (Distroferric Red Latosol, LVd) from a slightly dissected unit in VRP (Soil Survey Staff, 2010) | | | | | | | | | | |
| A | 0–0.3 | 83 | 82 | 56 | 770 | 15 | 245 | 1.72 | 1.20 | 5YR 3/3 |
| B | 0.3–0.5 | 72 | 90 | 40 | 740 | 20 | 240 | 1.36 | 1.06 | 5YR 3/3.5 |
| B/C | 0.5–0.9 | 64 | 58 | 46 | 790 | 20 | 190 | 1.88 | 1.25 | 7.5YR 5/3 |
| 5 - Rhodic Hapludox (Distroferric Red Latosol, LVd) from a moderately dissected unit in VRP (Soil Survey Staff, 2010) | | | | | | | | | | |
| A | 0–0.3 | 46 | 33 | 36 | 870 | 10 | 120 | 2.37 | 1.40 | 7YR 4/5 |
| B | 0.3–0.5 | 71 | 64 | 56 | 740 | 20 | 240 | 189 | 1.08 | 7.5YR 4/5 |
| B/C | 0.3–0.9 | 74 | 72 | 54 | 760 | 10 | 230 | 1.75 | 1.19 | 7.5YR 4/5 |
| 6 - Typic Kandiudalf (Red–Yellow Argisol, PVA) from a highly dissected unit in VRP (Soil Survey Staff, 2010) | | | | | | | | | | |
| Ap | 0-0.2 | 35 | 31 | 14 | 900 | 60 | 40 | 1.92 | 1.5 | 10YR 4/6 |
| B/C | 0.2-0.7 | 100 | 87 | 27 | 740 | 240 | 20 | 1.95 | 1.63 | 8YR 3/6 |

[1,2]Weathering indices: $K_i = 1.7 \times \%SiO_2/\%Al_2O_3$; $K_r = 1.7 \times \%SiO_2/[\%Al_2O_3 + (0.6325 \times \%Fe_2O_3)]$.

$Fe_2O_3$ and $K_i$ ($r = -0.86$, $p<0.05$).

$Fe_2O_3$ and $K_r$ ($r = -0.92$, $p<0.05$).

(198–228 g kg$^{-1}$) were those of basaltic soils from SG and the lowest (14–57 g kg$^{-1}$) those of sandy soils from VRP. Based on the results of sulfuric digestion tests, clayey and very clayey soils from SG were ferric ($18 \leq Fe_2O_3 < 36\%$), while sandy clay loam and sandy loam soils from VRP were hypoferric ($Fe_2O_3 < 8\%$) (Embrapa, 2013). These results are similar to those found by other authors who identified $Fe_2O_3$ variability as the main pedoindicator for soils from contrasting parent materials (Cunha et al., 2005; Carvalho Filho et al., 2015; Camargo et al., 2016).

As shown in Table 1, the weathering indices $K_i$ and $K_r$ calculated from the mole ratios of $SiO_2$, $Al_2O_3$, and $Fe_2O_3$ were influenced by differences in lithology and landscape dissection. Thus, $K_i$ and $K_r$ for basaltic Latosols (LVef_SG) were 0.48–1.69 and 0.35–1.13, respectively, and hence lower than those for sandy Latosols (LVd_VRP) and Argisols (PVA_VRP): 1.36–2.37 and 1.02–1.63, respectively. It was a result of the abundance of $Fe_2O_3$ in basaltic rocks and their easier weathering (Campos et al., 2007). The high degree of weathering was consistent with the loss of silica from soils, as implied by the negative correlations of $Fe_2O_3$ content with $K_i$ ($r = -0.86$, $p < 0.05$) and $K_r$ ($r = -0.92$, $p < 0.05$). These correlations indicate that both indices decreased with increasing $Fe_2O_3$ and $Al_2O_3$ contents but decreasing $SiO_2$ content (Embrapa, 2013). Also, the fact that $K_r$ was lower than 0.7 allowed the soils from SG to be classified as oxidic and those from VRP as kaolinitic.

In morphogenetic and pedogenetic terms, the variability in $Fe_2O_3$ content, $K_i$, and $K_r$ was related to the degree of landscape dissection (Table 1). Thus, $K_i$ and $K_r$ were lower in soils from Hd landscape units, where concave and convex landforms prevailed (Fig. 1b), than they were in soils from Sd units at the top heights, with convex and linear landforms and less markedly weathered soil. Queiroz Neto and Pellerin (1994) found Hd units to be strongly weathered, less stable steep V-shaped valleys where morphogenesis prevailed over pedogenesis. According to Cunha et al. (2005), top surfaces are more stable and have

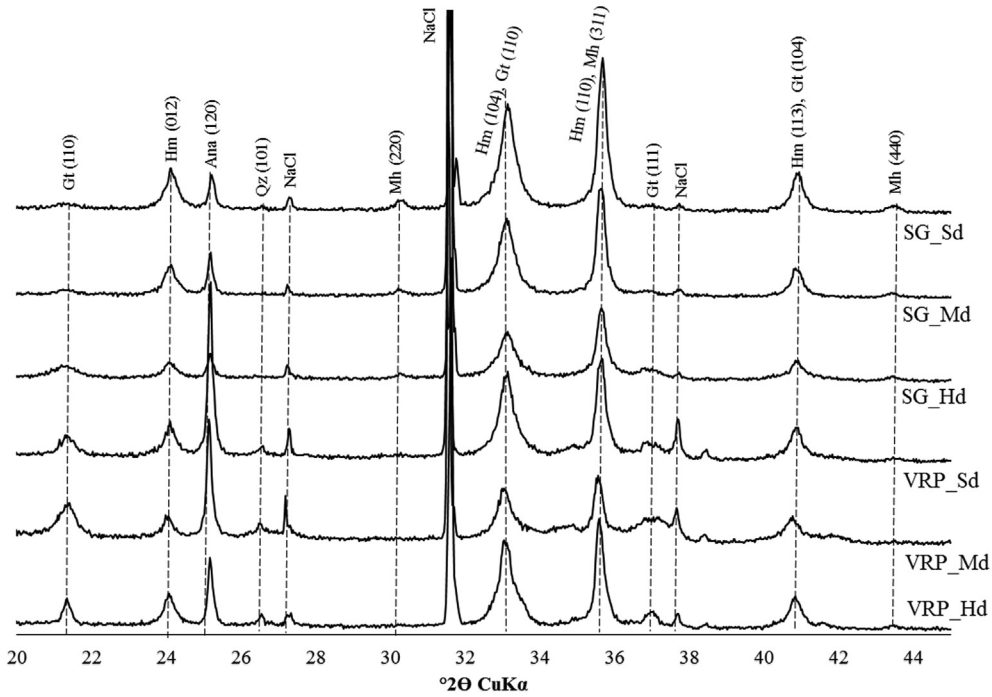


**Fig. 2.** XRD patterns for six profiles representing the basaltic soils in the Serra Geral formation (SG) and sandstone soils in the Vale do Rio do Peixe formation (VRP). Sd, Md, and Hd denote slightly, moderately, and highly dissected units, respectively. Gt, goethite. Hm, hematite. Qz, quartz. Mh, maghemite. NaCl, sodium chloride.

more developed and stable soils than more unstable surfaces. It was also the case here, where LVef_SG and PVA_VRP soils in the Hd units were younger ($K_i$ and $K_r$ were both greater than unity), shallow, and with lithic contact (C horizon) within the top 2 m.

Color hues ranged from 2.5 YR to 10 YR, and no soil was purely red or yellow (Table 1). Color parameters clearly reflect the almost exclusive legacy of the parent material to soil color. Thus, soil color is an accurate indicator of the presence of iron oxides (Torrent, 2005; Viscarra Rossel et al., 2010) and also of components of the parent material. The high variability of $Fe_2O_3$ contents requires identifying the iron oxides present in the soil, particularly hematite and goethite, not only because they give soils their color but also because their presence is related to soil formation environment (Schwertmann, 1993).

### 3.2. Identification of iron oxides

#### 3.2.1. X-ray diffraction

The XRD patterns for iron oxides in the clay fraction revealed the presence of antiferromagnetic minerals such as Hm and Gt, and ferrimagnetic minerals such as Mh. The latter, however, was only found in some soils from SG (Fig. 2; Table 2). The wide range of Hm and Gt contents (1–120 and 1–97 g kg$^{-1}$, respectively) reflects the diversity of parent materials; also, the prevalence of these oxides was a result of the intrinsic nature of rocks. This assumption is supported by the significant differences in Hm and Gm contents between soils in the lithological sections. The average contents and their ranges are consistent with previous results of Camargo et al. (2016) and Barbieri et al. (2013) in similar experiments conducted at a smaller scale in the same region.

Despite their concomitance, Hm and Gt were significantly related ($p < 0.05$) to the nature of the parent material (Table 2). The abundance of Hm and Gt, which jointly accounted for 89% of the overall iron oxide content, led to the $Fe_2O_3$ content of the basaltic soils (> 180 g kg$^{-1}$) being 54% higher than that of sandy soils. According to Schwertmann and Taylor (1989), the increased Fe content of basalt, in combination with free drainage, favors Hm formation. It was indeed the case here judging by strong XRD peaks for Hm and only moderate peaks for Gt in soils from SG (Fig. 2).

The degree of landscape dissection significantly influenced ($p < 0.05$) Hm content, concentrating on Sd units (Table 2; Fig. 2), where soils are more developed and have good internal drainage. Gt did not respond to the degree of dissection, but the increase in Gt concentration towards Hd units indicates a better environmental condition to its growth, a fact also observed by Coventry and Williams (1984) in a highly dissected landscape with poor drainage. Motta et al. (2002) stated that in the occurrence of highly dissected units in the most depressed landscape regions, soils undergo a reduction process in humid pedoenvironments favorable to Gt stability and preferential to Hm dissolution (Macedo and Bryant, 1987).

#### 3.2.2. Diffuse reflectance spectroscopy

The use of DRS in ADFE also indicated the coexistence of Hm and Gt in soils, and their persistence is determined by lithology and landscape dissection units (Fig. 3). It occurs because Fe oxides are the main inorganic constituents to determine soil color (Resende, 1976; Schwertmann, 1993; Viscarra Rossel et al., 2010) and their occurrence and persistence depend on the parent material and environmental conditions. In the visible region (400–780 nm), a typical zone of Fe oxides (Sherman and Waite, 1985), reflectance intensities and spectral curve features indicated a wide variation in Hm and Gt content, indicating a distinct preference for their formation, subordinated to lithologic and landscape characteristics.

The reflectances separated the lighter and yellowish (7YR, 7.5YR, 8YR, and 10YR, Tab. 1) LVd and PVA of VRP from the darker LVef and more intense red (2.5YR and 5YR, Tab. 1) of SG (Fig. 3). The low $Fe_2O_3$ contents and better performance of Gt affected the increase of reflectivity in soils from VRP because yellow soils have a lower light absorption potential when compared to red soils typical of Hm (Fernandes et al., 2004). On the other hand, the sharp decay of the spectral curve defined SG soils, where a more pronounced concavity of around 530 nm indicates a predominance of Hm, justifying the lower reflectance, considering its higher light absorption capacity.

The DRS technique separated soils by dissection units whose reflectance decreased in the visible range in the following sequence: Hd > Md > Sd. It can be attributed to the fact that landscape

**Table 2**
Descriptive statistics for goethite (Gt) and hematite (Hm) as determined by XRD in 200 soils samples in slightly (Sd), moderately (Md), and highly dissected (Hd) units of the Serra Geral (SG) and Vale do Rio Peixe (VRP) formations.

| [1]Mineral | Soil dissection | Mean | Overall mean | Min. | Median | Max. | Skew. | Kurt. | SD | CV (%) |
|---|---|---|---|---|---|---|---|---|---|---|
| Basalt –SG | | | | | | | | | | |
| Hm | LVef_Sd | 59ab | 48A | 16 | 47 | 120 | 0.68 | −0.7 | 33 | 55 |
| | LVef_Md | 41b | | 6 | 41 | 70 | −0.2 | −0.77 | 18 | 43 |
| | LVef_Hd | 44a | | 11 | 40 | 84 | 0.76 | 1.24 | 30 | 70 |
| Gt | LVef_Sd | 44a | 41A | 10 | 34 | 87 | 0.37 | −1.36 | 27 | 62 |
| | LVef_Md | 40a | | 8 | 37 | 97 | 0.66 | 0.19 | 22 | 57 |
| | LVef_Hd | 34a | | 21 | 28 | 60 | 1.54 | 2.12 | 18 | 52 |
| Sandstone –VRP | | | | | | | | | | |
| Hm | LVd_Sd | 16a | 16B | 2 | 19 | 33 | −0.01 | −1.55 | 11 | 69 |
| | LVd_Md | 17a | | 1 | 14 | 88 | 2.57 | 9.6 | 16 | 94 |
| | PVA_Hd | 14a | | 2 | 12 | 30 | 0.27 | −1.08 | 8 | 61 |
| Gt | LVd_Sd | 17a | 19B | 5 | 15 | 34 | 0.45 | −0.68 | 9 | 53 |
| | LVd_Md | 18a | | 3 | 18 | 37 | 0.39 | −0.61 | 9 | 53 |
| | PVA_Hd | 20a | | 1 | 18 | 55 | 1.24 | 2.51 | 10 | 49 |

[1] Content in g $kg^{-1}$. LVef, Eutroferric Red Latosol. LVd, Dystrophic Red Latosol. PVA, Red–Yellow Argisol. SD, standard deviation. CV, coefficient of variation. Min., minimum value. Max., maximum value. Skew, skewness. Kurt., kurtosis. Means followed by the same uppercase letter in the column or lowercase letter in the row were not significantly different by the Tukey's test at 5% probability level.

dissection (Coventry et al., 1983) and relief (Curi and Franzmeier, 1984; Dotto et al., 2014; Camargo et al., 2013) is the main factor of soil formation at the local scale to determine the type of Fe oxides present. Thus, less differentiated curves and more pronounced concavities represented the most stable relief of SG, while contrary reasons pointed out the rugged landscape of VRP. Thus, the spectral behavior indicated that soils in the same lithological section might present different reflectance intensities subordinated to landscape dissections.

The results of sulfuric extracts (Table 1) and XRD patterns (Table 2; Fig. 2) in combination exposed a relationship of the spectral data (Fig. 3) with soil weathering, parent material, and landscape dissection. Thus, the decreased reflectance of basaltic soils in Sd units, which is consistent with $K_i$ and $K_r$ values, and with the increased $Fe_2O_3$ contents, is also apparent from DRS results. Therefore, both techniques led to identical interpretations. Also, the results suggest that soil color is an effective pedoenvironmental indicator strengthening the potential of DRS for environmental characterization.

### 3.2.3. *XRD versus DRS for characterizing iron oxides in surface soils*

In the 200 surface samples, Hm and Gt contents spanned the ranges of 1–120 and 1–97 g $kg^{-1}$, respectively, according to XRD, and 4–109 and 1–90 g $kg^{-1}$, respectively, according to DRS (Table 3). Based on Student's *t*-test, the contents were not significantly different ($p > 0.05$) among landscape dissection levels regardless of the used technique, and only those in Gt differed significantly with DRS. Probably, in those situations where the proportions of the two oxides are much higher and the prevalence of Hm is favored as a result, DRS may be unable to detect Gt – hence the differences between both techniques.

The origin values of linear regression (8.04 for Hm_XRD and 4.22 for Gt_XRD) were very high (Fig. 4ab), corroborating other studies (Bahia et al., 2015; Camargo et al., 2016). This result supports the idea that under certain circumstances XRD may be less efficient to detect little amounts of Hm and Gt oxides in the soil (Kämpf and Curi, 2000; Schaefer et al., 2008). This phenomenon was observed in Gt content (Fig. 2), which was almost imperceptible in the slightly dissected units

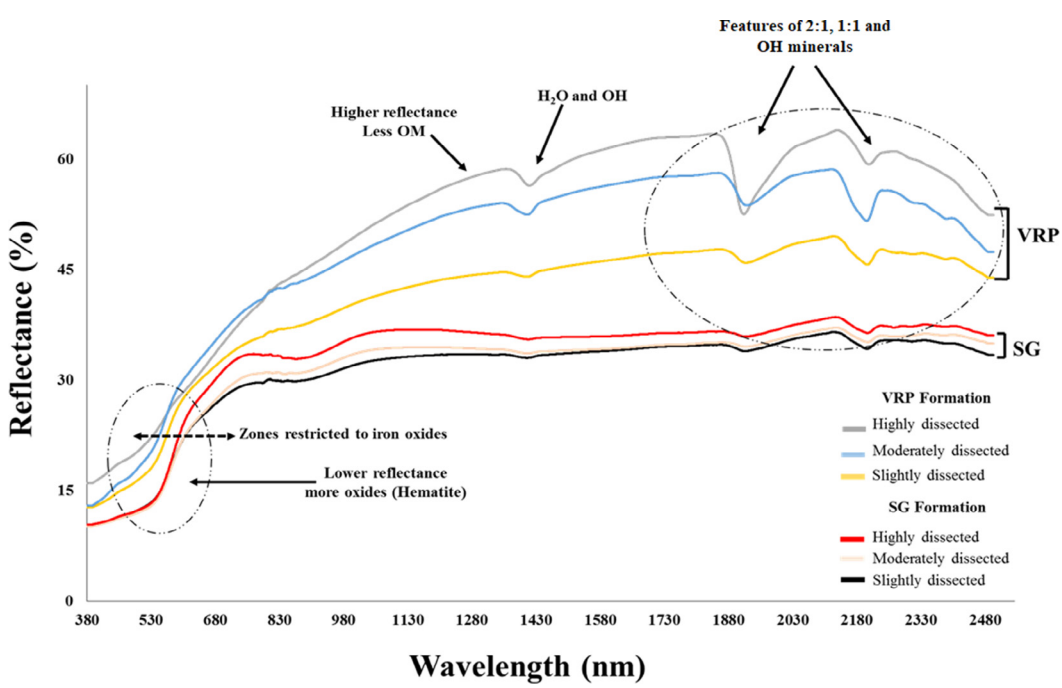


**Fig. 3.** Diffuse reflectance spectra for six soil profiles typical of three different dissection levels in Serra Geral (SG) and Vale do Rio Peixe (VRP) formations, Western Paulista Plateau.

**Table 3**
Descriptive statistics for Hm and Gt contents as determined by XRD and estimated by DRS in 200 soil samples from the Western Paulista Plateau.

| Technique | Unit | Overall mean* | Mean* | Minimum | Median | Maximum | Skewness | Kurtosis | SD[1] | CV[2] |
|---|---|---|---|---|---|---|---|---|---|---|
| Hm_XRD[3] | Sd | | 30.6 a | 2 | 23 | 120 | 1.74 | 2.70 | 30 | 99 |
| | Md | 26.3 A | 27.1 a | 1 | 18 | 121 | 1.60 | 2.75 | 25 | 92 |
| | Hd | | 14.9 a | 2 | 9 | 84 | 2.75 | 9.09 | 17 | 117 |
| Hm_DRS[3] | Sd | | 33.9 a | 4 | 26 | 111 | 1.44 | 1.24 | 28 | 82 |
| | Md | 31.8 A | 33.8 a | 5 | 22 | 101 | 0.98 | −0.15 | 26 | 77 |
| | Hd | | 21.7 a | 6 | 15 | 94 | 2.47 | 5.28 | 22 | 103 |
| Gt_XRD[3] | Sd | | 29.5 a | 5 | 20 | 87 | 1.34 | 0.71 | 23 | 77 |
| | Md | 26.7 A | 26.2 a | 1 | 21 | 97 | 1.93 | 4.66 | 18 | 68 |
| | Hd | | 22.6 a | 3 | 21 | 75 | 2.29 | 8.64 | 13 | 60 |
| Gt_DRS[3] | Sd | | 24.0 a | 1 | 16 | 78 | 1.50 | 1.73 | 18 | 76 |
| | Md | 22.3B | 22.8 a | 1 | 17 | 75 | 1.33 | 0.97 | 17 | 74 |
| | Hd | | 17.1 a | 2 | 16 | 44 | 1.05 | 3.42 | 8 | 48 |

* Means followed by the same uppercase letter in the column or lowercase letter in the row were not significantly different by the Tukey's test at 5% probability level
[1] Standard deviation.
[2] Coefficient of variation (%).
[3] g kg$^{-1}$.

of basaltic soils, while DRS efficiency has been registered even in soils with low Fe contents (< 0.05%), which is the minimum detection limit of conventional XRD (Barrón et al., 2000; Balsam et al., 2014).

The prediction accuracy of regression models (Fig. 4(a and, b)), assuming high values of $R^2$ and RPD and low of RMSE and SDE, classified the models as excellent (Chang et al., 2001). Negative and positive ME values showed that DRS underestimates Hm and overestimates Gt. However, it is not a limiting factor of DRS in estimating Fe oxides, as confirmed by a strong significant correlation between XRD and DRS found for Hm ($R^2 = 0.82$; $p < 0.01$) and Gt ($R^2 = 0.61$; $p < 0.01$). This result is consistent of those reported by Bahia et al. (2015) for Hm ($R^2 = 0.99$; $p < 0.01$) and Gt ($R^2 = 0.79$; $p < 0.01$), Camargo et al. (2016) for Hm ($R^2 = 0.70$; $p < 0.01$) and Gt ($R^2 = 0.71$; $p < 0.01$), and Cezar et al. (2013) for the correlation between the synthetic Hm content and its reflectance factor ($R^2 = 0.99$).

### 3.3. Geostatistical analysis and mapping of iron oxides

According to Warrick and Nielsen (1980) criteria for coefficients of variation, those for Hm and Gt (48–117%) exceed 24% and, therefore, the variability in XRD (Table 2) and DRS values (Table 3) for the two oxides was high. However, this descriptive statistics may not accurately reflect the facts, as it refers to the overall mean of a dataset (Siqueira et al., 2015). Consequently, it is preferable to use geostatistical kriging tools instead as they operate on local means (Siqueira et al., 2015; Teixeira et al., 2018).

In both techniques, Hm and Gt presented spatial dependence described by the spherical model (Fig. 5). This model is common in the investigation of soil phenomena (Vieira, 2000) with more abrupt variations (Isaaks and Srivastava, 1989), confirming the influence of geology and the degree of landscape dissection. In fact, the degree of spatial dependence (DSD) classified the spatialization of oxides as moderate (25 < DSD > 75%), revealing that the spherical model explains most of the variance of the experimental data, with $R^2 > 0.6\%$. As assigned herein, Zheng et al. (2009) cited that moderate and high special dependences are associated with soil variables controlled by the parent material, such as mineralogy.

Hm presented a lower spatial variability when compared to Gt, expressed by the range (*a*) values (Fig. 5), which is an indicative parameter of the spatial distance that the variables are correlated (Tabi and Ogunkunle, 2007). Ranges of 72 and 42 km (XRD) for Hm and 81 and 29 km (DRS) for Gt suggest that the variability occurred at different

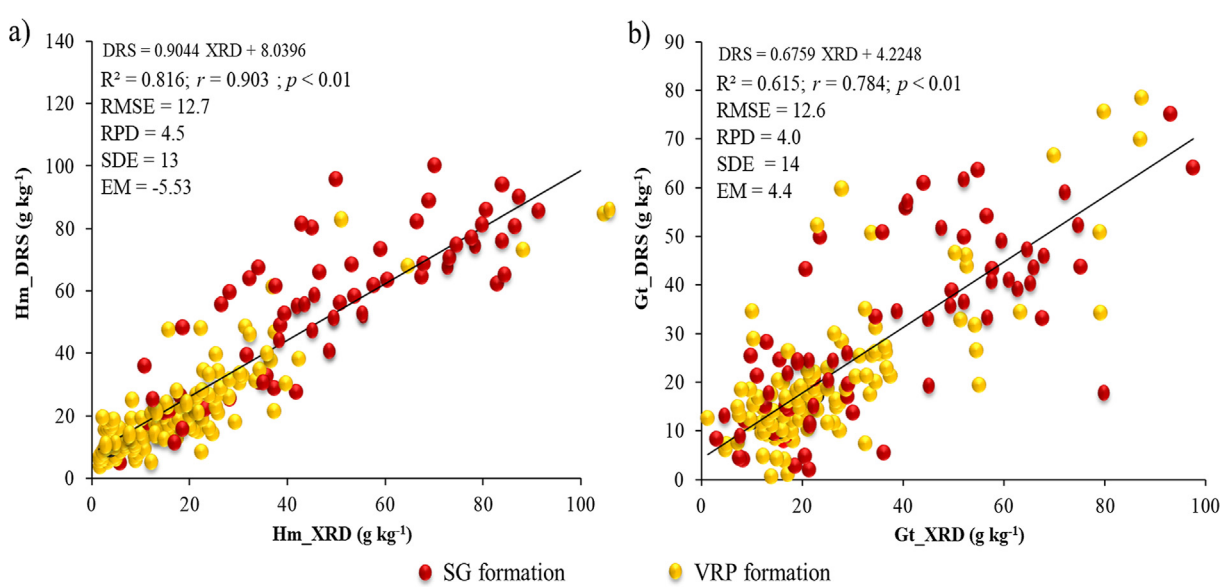


**Fig. 4.** Regression models for (*a*) hematite as determined by X-ray diffraction (XRD) and estimated by diffuse reflectance spectroscopy (DRS); and (*b*) goethite as determined by XRD and estimated by DRS.

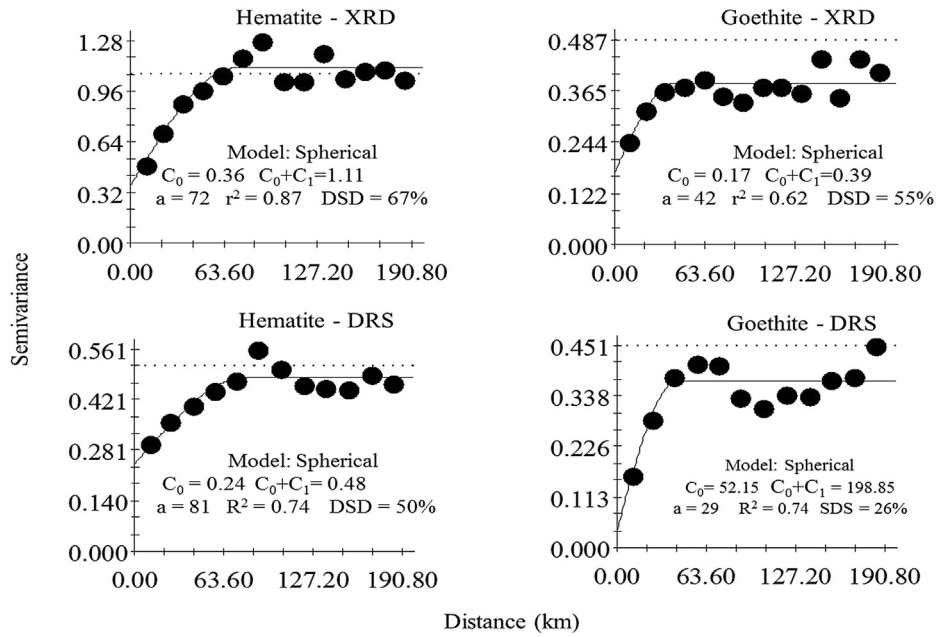


**Fig. 5.** Variograms for hematite and goethite as obtained from XRD and DRS data for soils from the lithostratigraphic units of the Western Paulista Plateau.

spatial scales, coordinated by lithological contrast and landscape dissections. Ranges from 20 to 1400 km found by Viscarra Rossel et al. (2010) and 24 m by Camargo et al. (2008a) indicate a higher spatial variability for Gt. The ubiquitous nature of this mineral formed in the soil solution from several Fe sources through a solution-nucleation crystallization process (Cornell and Schwertmann, 2003) justifies its sensitivity to environmental changes in relation to Hm, which is formed in the solid phase from ferrihydrite (Inda and Kämpf, 2005).

The spatial patterns of Hm and Gt by XRD and DRS are shown in Fig. 6(a–f). The XRD maps presented more definite delimitations for Hm (Fig. 6a), while the larger indentations and less defined limits of isolines confirm a higher spatial variability for Gt, confirming the lower ranges found in Fig. 5. The spatial pattern illustrated the lithological contrast (Fig. 6(a–g)), which is consistent with the geological map of Fernandes et al. (2007) (Fig. 6g), where basaltic soils were concentrated in the peripheries of SG, and the large central spot referred to sandstones of VRP. Thus, the XRD and DRS maps indicated the spatialization of Hm and Gt, indicators of soils from parent materials with low and high Fe contents, respectively.

In the estimates of Hm, the lowest contents, between 4 and

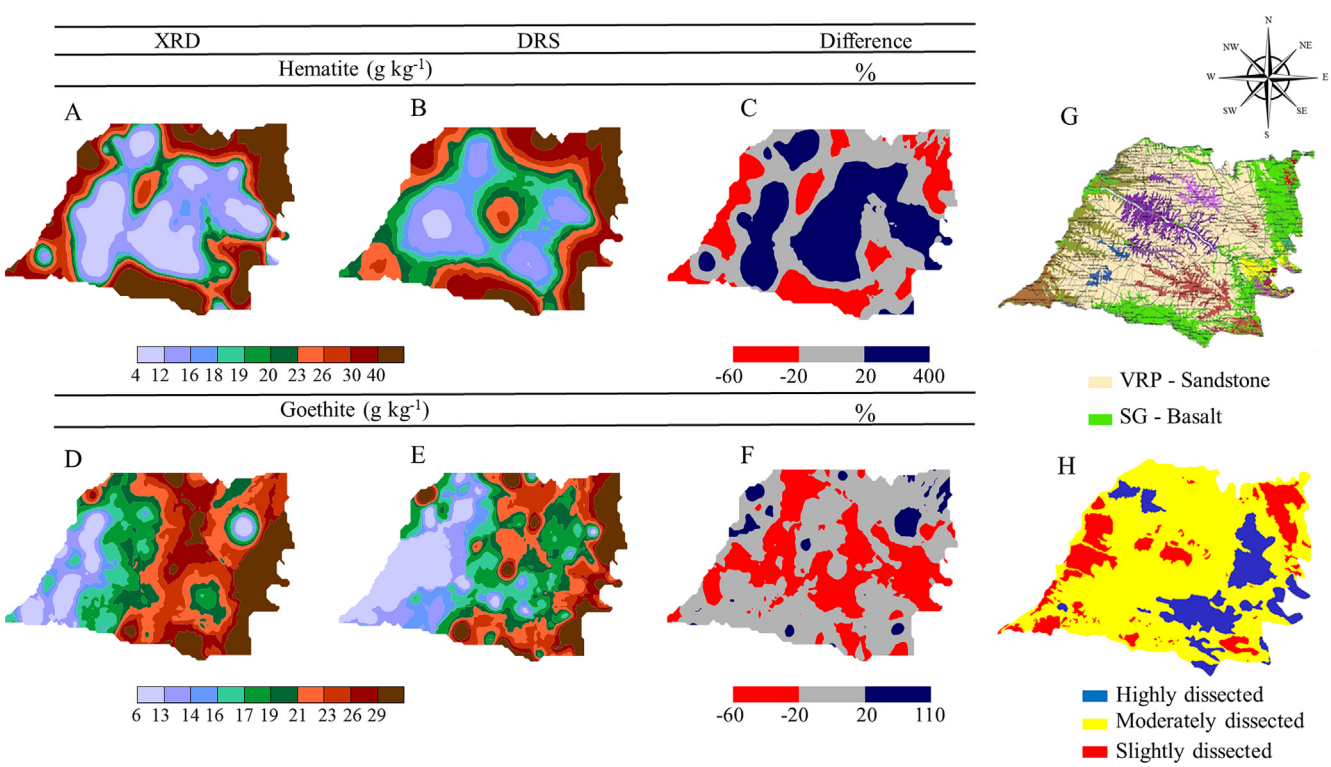


**Fig. 6.** Spatial patterns for hematite as estimated by XRD (*a*) and DRS (*b*), and validation between the two techniques (*c*). Spatial patterns for goethite as estimated by XRD (*d*) and DRS (*e*), and validation between the two techniques (*f*). Geological maps (*g*) and landscape dissection units (*h*).

16 g kg$^{-1}$ (Fig. 6(a and, b)), occurred in the central region under the domain of sedimentary rocks and the highest contents at the edges of WPP. A similar observation was carried out by Camargo et al. (2008a, 2008b) in a basalt/sandstone transect, where Hm was the main pedoindicator of the basaltic soils and Gt of sandstone soils, with a lower total Fe content. Therefore, both XRD and DRS discriminated sandstone (center) and basaltic (edges) soils by the amplitude of Fe oxides, clearly showing a low Fe concentration in the center of the map, in the essentiality of sandstones of VRP.

The DRS technique underestimated the contents of 23 to 40 g kg$^{-1}$ for 19 to 23 g kg$^{-1}$ of Hm in the west and southeast direction, especially in the edges under the domain of basaltic soils. This region corresponds in large part to Sd pedoenvironments, in which the enriched $Fe_2O_3$ (> 210 g kg$^{-1}$ $Fe_2O_3$, Table 1) of soils saturated the red color (hue 2.5 YR, Table 1) by the almost absolute presence of Hm, which constituted up to 33% of $Fe_2O_3$ of soils from SG. According to Fernandes et al. (2004), it would be a limitation of DRS in soil samples with Hm content around 15% of total Fe oxides. Bahia et al. (2015) also addressed this problem in soils with > 18% $Fe_2O_3$, in which Hm was the predominant Fe oxide.

Map validations (Fig. 6(g–h)) showed that the spatial pattern of Hm, although similar, had higher overestimated errors (> 20% of XRD values) in the range from 4 to 12 g kg$^{-1}$ (Fig. 6(a and, b)). From 21 to 29 g kg$^{-1}$, Gt contents were underestimated at 16 to 19 g kg$^{-1}$ by DRS, mainly in the central region (Fig. 6e). Basaltic flows among sandstones (Fernandes et al., 2007) overestimated Hm in sandstone environments due to the mixture of soils. Water table fluctuation, given the drainage networks that cut VRP, favors redox cycles, precipitating Fe in the wet season and its conversion into Hm in the dry season (Coventry et al., 1983), underestimating Gt by DRS. Macedo and Bryant (1987) recorded in dissected environments a change from dark red to yellow in Oxisols of the Brazilian Central Plateau due to water table fluctuation.

The DRS technique was more assertive in the spatial pattern of Gt (Fig. 6h). Assuming a 20% error, it can be used in 89 and 53% of the WPP area to estimate Gt and Hm, respectively, under study conditions (Fig. 6g). Fe oxides obtained by DRS were underestimated by 37% and overestimated by 23% of the total WPP area in relation to XRD. For Hm, the over- and underestimated values of DRS were 3.4 and 23%, respectively. The results confirm the acceptable accuracy of DRS in the estimation of Hm and Gt in large areas with geomorphological complexity, large variation of total Fe, and type of predominant Fe oxides.

From the pedometrics point of view, there is a need for new methods that make more efficient the mapping of soil attributes (Viscarra Rossel et al., 2010; Marques et al., 2014; Siqueira et al., 2015; Teixeira et al., 2018). The good correlations obtained for Hm and Gt, determined by XRD and estimated by DRS, indicate the potential and viability of this method in characterizing these Fe oxides in a large number of ADFE samples, quickly, with a low cost, and in large areas. This technique can assist the conventional methods of mapping, detailed survey of soils, and covariate attributes of the oxidic mineralogy of tropical environments since the estimated results and spatial pattern were very close to those observed.

## 4. Conclusions

The sandstone/basalt lithological contrast and the degree of landscape dissection are the main factors governing the prevalence and spatial variability of Hm and Gt in soils from the Western Paulista Platform. Iron oxides in the clay fraction exhibit spatial variability over large areas and are robust indicators of geological diversity and landscape dissection in environments with soils containing large amounts of iron oxides. Goethite is the most spatially variable oxide in the Plateau. Based on the spatial pattern of differences between DRS and XRD measurements, red color saturation makes the DRS technique less useful for quantifying Hm in soils with high Fe oxide contents. The maps indicate the sensitivity of XRD and DRS techniques to represent Hm and Gt spatial variability patterns. Gt was more sensitive to landscape dissection while Hm sensitive to lithology. Thus, the DRS technique is efficient in characterizing the spatial variability of these soil oxides in large areas, even considering the complex relations between soil and landscape.

## Acknowledgments

We thank the São Paulo Research Foundation (FAPESP), Brazil for funding this study (Process no. 402796/2016-0; Doctorate fellowship no. 2017/01704-2 and BEPE, Spain, no. 2018/15694-1). To Coordination for the Improvement of Higher-Level Personnel (CAPES, Brazil, proc. no. 149940), PROPE/UNESP (Pro-Rector of Research of the São Paulo State University, Call no. 15/2014) and the National Council for Scientific and Technological Development (CNPq, Brazil) for granting the scholarships.

## References

Arenas-Lago, D., Vega, F.A., Silva, L.F., Andrade, M.L., 2014. Copper distribution in surface and subsurface soil horizons. Environ. Sci. Pollut. Res. Int. 21, 10997–11008. https://doi.org/10.1007/s11356-014-3084-4.

Bahia, A.S.R.S., Marques Jr., J., Siqueira, D.S., 2015. Procedures using diffuse reflectance spectroscopy for estimating hematite and goethite in Oxisols of São Paulo, Brazil. Geoderma 5, 150–156. https://doi.org/10.1016/j.geodrs.2015.04.006.

Balsam, W., Ji, J., Renock, D., Deaton, B.C., Williams, E., 2014. Determining hematite content from NUV/Vis/NIR spectra: limits of detection. Am. Mineral. 99, 2280–2291. https://doi.org/10.2138/am-2014-4878.

Barbieri, D.M., Marques Jr., J., Pereira, G.T., La Scala, N., Siqueira, D.S., Panosso, A.R., 2013. Comportamento dos óxidos de ferro da fração argila e do fósforo adsorvido, em diferentes sistemas de colheita de cana-de-açúcar. Rev. Bras. Cienc. Solo 37, 1557–1568. https://doi.org/10.1590/s0100-06832013000600012.

Barrón, V., Mello, J.W.V., Torrent, J., 2000. Caracterização de óxidos de ferro em solos por Espectroscopia de Reflectância Difusa. In: Novais, R.F., Alvarez, V.H., Schaefer, C.E.G.R. (Eds.), Tópicos em ciência do solo. Sociedade Brasileira de Ciência do Solo, Viçosa, pp. 139–162.

Camargo, L.A., Marques, J., Pereira, G.T., Alleoni, L.R.F., Bahia, A.S.R.S., Teixeira, D.D.B., 2016. Pedotransfer functions to assess adsorbed phosphate using iron oxide content and magnetic susceptibility in an Oxisol. Soil Use Manage. 32, 172–182. https://doi.org/10.1111/sum.12255.

Camargo, L.A., Marques Jr., J., Pereira, G.T., 2013. Mineralogy of the clay fraction of Alfisols in two slope curvatures: III – Spatial variability. Rev. Bras. Cienc. Solo 37, 295–306. https://doi.org/10.1590/s0100-06832013000200001.

Camargo, L.A., Marques Jr., J., Pereira, G.T., Horvat, R.A., 2008a. Spatial variability mineralogical of an Oxisol under different landforms. I. Mineralogy of the clay fraction. Rev. Bras. Cienc. Solo 32, 2269–2277. https://doi.org/10.1590/S0100-06832008000600006.

Camargo, L.A., Marques Jr., J., Pereira, G.T., Horvat, R.A., 2008b. Spatial variability mineralogical of an Oxisol under different landforms. II. Spatial correlation between mineralogy and aggregates. Rev. Bras. Cienc. Solo 32, 2279–2288. https://doi.org/10.1590/S0100-06832008000600007.

Cambardella, C.A., Moorman, T.B., Novak, J.M., Parkin, T.B., Karlen, D.L., Turco, R.F., Konopka, A.E., 1994. Field-scale variability of soil properties in Central Iowa Soil. Soil Sci. Soc. Am. J. 58, 1501–1508. https://doi.org/10.2136/sssaj1994.03615995005800050033x.

Campos, M.C.C., Marques Jr., J., Pereira, G.T., Montanari, R., Camargo, L.A., 2007. Relações solo-paisagem em uma litossequência arenito-basalto na região de Pereira Barreto, SP. Revista Rev. Bras. Cienc. Solo 31, 519–529. https://doi.org/10.1590/S0100-06832007000300012.

de Carvalho Filho, A., Inda, A.V., Fink, J.R., Curi, N., 2015. Iron oxides in soils of different lithological origins in Ferriferous Quadrilateral (Minas Gerais, Brazil). Appl. Clay Sci. 118, 1–7. https://doi.org/10.1016/j.clay.2015.08.037.

Chang, C.W., Laird, D.A., Mausbach, M.J., Hurburgh, C.R., 2001. Near-infrared reflectance spectroscopy-principal components regression analyses of soil properties. Soil Sci. Soc. Am. J. 65, 480–490. https://doi.org/10.2136/sssaj2001.652480x.

Cezar, E., Nanni, M.R., Chicati, M.L., de Souza Júnior, I.G., Costa, A.C.S., 2013. Uso de dados espectrais para estimar a relação entre óxidos de ferro e minerais 2:1 com suas respectivas reflectâncias. Semina: Ciênc Agrár. 34, 1479–1492. https://doi.org/10.5433/1679-0359.2013v34n4p1479.

Cornell, R.M., Schwertmann, U., 2003. The Iron Oxides: Structure, Properties, Reactions, Occurrences and Uses, second ed. Wiley-VCH Verlag GmbH & Co, KGaA, Weinheim.

Coventry, R.J., Taylor, R.M., Fitzpatrick, R.W., 1983. Pedological significance of the gravels in some red and grey earths of central north Queensland. Aust. J. Soil Res. 21, 219–240. https://doi.org/10.1071/SR9830219.

Coventry, R.J., Williams, J., 1984. Quantitative relationships between morphology and the current soil hydrology, in some Alfisols in semi-arid tropical Australia. Geoderma 33, 191–218.

Cunha, P., Marques Jr., J., Curi, N., Pereira, G.T., Lepsch, I.F., 2005. Superfícies geomórficas e atributos de Latossolos em uma sequência arenítico-basáltica da região de Jaboticabal (SP). Rev. Bras. Cienc. Solo 29, 81–90. https://doi.org/10.1590/

S0100-06832005000100009.
Curi, N., Franzmeier, D.P., 1984. Toposequence of Oxisols from the central plateau of Brazil. Soil Sci. Soc. Am. J. 48, 341–346. https://doi.org/10.2136/sssaj1984.03615995004800020024x.
Dalmora, A.C., Ramos, C.G., Querol, X., Kautzmann, R.M., Oliveira, M.L.S., Taffarel, S.R., Moreno, T., Silva, L.F., 2016a. Nanoparticulate mineral matter from basalt dust wastes. Chemosphere 144, 2013–2017. https://doi.org/10.1016/j.chemosphere.2015.10.047.
Dalmora, A.C., Ramos, C., Oliveira, M., Teixeira, E., Kautzmann, R., Taffarel, S., De Brum, I., Silva, L.F., 2016b. Chemical characterization, nano-particle mineralogy and particle size distribution of basalt dust wastes. Sci. Total Environ. 539, 560–565. https://doi.org/10.1016/j.scitotenv.2015.08.141.
Daniels, R.B., Gamble, E.F., Cady, J.G., 1971. The relation between geomorphology and soil morphology and genesis. Adv. Agron. 23, 51–87. https://doi.org/10.1016/S0065-2113(08)60150-9.
Dotto, A.C., Dalmolin, R.S.D., Pedron, F.A., ten Caten, A., Ruiz, L.F.C., 2014. Mapeamento digital de atributos: granulometria e matéria orgânica do solo utilizando espectroscopia de reflectância difusa. Rev. Bras. Cienc. Solo 38, 1663–1671. https://doi.org/10.1590/S0100-06832014000600001.
Duiker, S.W., Rhoton, F.E., Torrent, J., Smeck, N.E., Lal, R., 2003. Iron (Hydr)Oxide crystallinity effects on soil aggregation. Soil Sci. Soc. Am. J. 67, 606. https://doi.org/10.2136/sssaj2003.6060.
Embrapa – Empresa Brasileira de Pesquisa Agropecuária, 2011. Manual de métodos de análise de solo. third ed. Embrapa Solos, Rio de Janeiro.
Embrapa – Empresa Brasileira de Pesquisa Agropecuária, 2013. Sistema brasileiro de classificação de solos. third ed. Embrapa Solos, Rio de Janeiro.
Embrapa – Empresa Brasileira de Pesquisa Agropecuária, 2016. Programa Nacional de Solos do Brasil – PronaSolos. https://www.embrapa.br/busca-de-publicacoes/-/publicacao/1054924/programa-nacional-de-solos-do-brasil-pronasolos (accessed 26 January 2019).
Ferrari, V., Taffarel, S.R., Espinosa-Fuentes, E., Oliveira, M.L.S., Saikia, B.K., Oliveira, L.F.S., 2019. Chemical evaluation of by-products of the grape industry as potential agricultural fertilizers. J. Cleaner Prod. 208, 297–306. https://doi.org/10.1016/j.jclepro.2018.10.032.
Fernandes, L.A., Castro, A.B., Basilici, G., 2007. Seismites in continental sand sea deposits of the Late Cretaceous Caiuá Desert, Bauru Basin, Brazil. Sediment. Geol. 199, 51–64. https://doi.org/10.1016/j.sedgeo.2005.12.030.
Fernandes, R.B.A., Barrón, V., Torrent, J., Fontes, M.P.F., 2004. Quantification of iron oxides in Brazilian latosols by diffuse reflectance spectroscopy. Rev. Bras. Ciênc. Solo 28, 245–257. https://doi.org/10.1590/S0100-06832004000200003.
Fitzpatrick, R.W., 1988. Iron compounds as indicators of pedogenic processes: examples from the Southern Hemisphere. In: Stucki, J.W., Goodman, J.M., Schwertmann, U. (Eds.), Iron in Soils and Clay Minerals. Springer, Dordrecht, pp. 351–396.
Guerrero, C., Viscarra Rossel, R.A., Mouazen, A.M., 2010. Special issue 'Diffuse reflectance spectroscopy in soil science and land resource assessment' preface. Geoderma 158, 1–2. https://doi.org/10.1016/j.geoderma.2010.05.008.
Inda Júnior, A.V., Kämpf, N., 2005. Variabilidade de goethita e hematita via dissolução redutiva em solos de região tropical e subtropical. Rev. Bras. Ciênc. Solo 29, 851–866. https://doi.org/10.1590/S0100-06832005000600003.
Isaaks, E.H., Srivastava, R.M., 1989. An Introduction to Applied Geostatistics. Oxford University Press, New York.
Kämpf, N., Curi, N., 2000. Óxidos de Ferro: indicadores de ambientes pedogênicos. In: Novais, R.F., Alvarez, V.H., Schaefer, C.E.G.R. (Eds.), Tópicos em Ciência do Solo. Sociedade Brasileira de Ciência do Solo, Viçosa, pp. 107–138.
Kämpf, N., Schwertmann, U., 1982. Goethite and hematite in a climosequence in Southern Brazil and their application in classification of kaolinitic soils. Geoderma 29, 27–39. https://doi.org/10.1016/0016-7061(83)90028-9.
Kubelka, P., Munk, F., 1931. Ein beitrag zur optic der farbanstriche. Z. Tech. Phys. 12, 593–620.
Macedo, J., Bryant, R.B., 1987. Morphology, mineralogy, and genesis of a hydrosequence of oxisols in Brazil. Soil Sci. Soc. Am. J. 51, 690–698. https://doi.org/10.2136/sssaj1987.03615995005100030025x.
Marques Jr., J., Alleoni, L.R.F., Teixeira, D.D.B., Siqueira, D.S., Pereira, G.T., 2015. Sampling planning of micronutrients and aluminium of the soils of São Paulo, Brazil. Geoderma Reg. 4, 91–99. https://doi.org/10.1016/j.geodrs.2014.12.004.
Marques Jr., J., Siqueira, D.S., Camargo, L.A., Teixeira, D.D.B., Barrón, V., Torrent, J., 2014. Magnetic susceptibility and diffuse reflectance spectroscopy to characterize the spatial variability of soil properties in a Brazilian Haplustalf. Geoderma 219–220, 63–71. https://doi.org/10.1016/j.geoderma.2013.12.007.
Martinello, K., Oliveira, M., Molossi, F., Ramos, C., Teixeira, E., Kautzmann, R., Silva, L.F., 2014. Direct identification of hazardous elements in ultra-fine and nanominerals from coal fly ash produced during diesel co-firing. Sci. Total Environ. 470–471, 444–452. https://doi.org/10.1016/j.scitotenv.2013.10.007.
Motta, P.E.F., Carvalho Filho, A., Ker, J.C., Pereira, N.R., 2002. Relações solo-superfície geomórfica e evolução da paisagem em uma área do Planalto Central Brasileiro. Pesq. Agropec. Bras. 37, 869–878. https://doi.org/10.1590/S0100-204X2002000600017.
Norrish, K., Taylor, R.M., 1961. The isomorphous replacement of iron by aluminum in soil goethites. J. Soil Sci. 12, 294–306. https://doi.org/10.1111/j.1365-2389.1961.tb00919.x.
Oliver, M.A., Webster, R., 2014. A tutorial guide to geostatistics: computing and modelling variograms and kriging. Catena 113, 56–69. https://doi.org/10.1016/j.catena.2013.09.006.
Peters, C., Dekkers, M.J., 2003. Selected room temperature magnetic parameters as a function of mineralogy, concentration and grain size. Phys. Chem. Earth 28, 659–694. https://doi.org/10.1016/S1474-7065(03)00120-7.
Poggere, G.C., Inda, A.V., Barrón, V., Kämpf, N., De Brito, A.D.B., Barbosa, J.Z., Curi, N., 2018. Maghemite quantification and magnetic signature of Brazilian soils with contrasting parent materials. Appl. Clay Sci. 161, 385–394. https://doi:10.1016/j.clay.2018.05.014.
Queiroz Neto, J.P., Pellerin, J., 1994. Solos e relevo no alto vale do rio do Peixe – Oscar Bressane (São Paulo – Brasil). Rev. Dep. Geogr. 777, 25–34. https://doi.org/10.7154/RDG.1994.0007.0002.
Resende, M., 1976. Mineralogy, Chemistry, Morphology and Geomorphology of Some Soils of Central Plateau of Brazil. 237 f. Thesis (PhD in Soil Science). Purdue University, Lafayette.
Robertson, G.P., 1998. GS+ Geostatistics for the Environmental Sciences: GS+ User's Guide. Gamma Design Software, Plainwell.
Saikia, B.K., Ward, C.R., Oliveira, M.L.S., Hower, J.C., Braga, M., Silva, L.F., 2014. Geochemistry and nano-mineralogy of two medium-sulfur northeast Indian coals. Int. J. Coal Geol. 121, 26–34. https://doi.org/10.1016/j.coal.2013.11.007.
Schaefer, C.E.G.R., Fabris, J.D., Ker, J.C., 2008. Minerals in the clay fraction of brazilian latosols (oxisols): a review. Clay Miner. 43, 137–154. https://doi.org/10.1180/claymin.2008.043.1.11.
Sánchez-Peña, N.E., Narváez-Semanate, J.L., Pabón-Patiño, D., Fernández-Mera, J.E., Oliveira, M.L., Da Boit, K., Tutikian, B., Crissien, T., Pinto, D., Serrano, I., Ayala, C., Duarte, A., Ruiz, J., Silva, L.F., 2018. Chemical and nano-mineralogical study for determining potential uses of legal Colombian gold mine sludge: experimental evidence. Chemosphere 191, 1048–1055. https://doi.org/10.1016/j.chemosphere.2017.08.127.
Scheinost, A., Chavernas, A., Barrón, V., Torrent, J., 1998. Use and limitations of second derivative diffuse reflectance spectroscopy in the visible to near-infrared range to identify and quantify Fe oxide minerals in soils. Clays Clay Miner. 46, 528–536. https://doi.org/10.1346/CCMN.1998.0460506.
Schwertmann, U., 1993. Relations between iron oxides, soil color, and soil formation. In: Bigham, J.M., Ciolkosz, E.J. (Eds.), Soil Color. Soil Science Society of America, Madison, pp. 51–69 (Special publication, 31).
Schwertmann, U., Taylor, R.M., 1989. Iron oxides. In: Dixon, J.B., Weed, S.B. (Eds.), Minerals in Soil Environments, second ed. Soil Science Society of America, Madison, pp. 379–438.
Sherman, D.M., Waite, T.D., 1985. Electronic spectra of $Fe^{3+}$ oxides and oxyhydroxides in the near infrared to ultraviolet. Am. Mineral. 70, 1262–1269.
Siqueira, D.S., Marques Jr., J., Pereira, G.T., Teixeira, D.D.B., Vasconcelos, V., Carvalho Júnior, O.A., Martins, E.S., 2015. Detailed mapping unit design based on soil—landscape relation and spatial variability of magnetic susceptibility and soil color. Catena 135, 149–162. https://doi.org/10.1016/j.catena.2015.07.010.
Smith, B., Sandwell, D., 2003. Accuracy and resolution of Shuttle Radar Topography Mission data. Geophys. Res. Lett. 30, 20–24. https://doi.org/10.1029/2002GL016643.
Soil Survey Staff, 2010. Keys to Soil Taxonomy, 11th ed. USDA-Natural Resources Conservation Service, Washington.
Surfer, S., 1999. 7.0. Contouring and 3D Surface Mapping for Scientist's Engineers. User's Guide. Golden software Inc, New York.
Tabi, F.O., Ogunkunle, A.O., 2007. Spatial variation of some soil physico-chemical properties of a alfisol in Southwestern Nigeria. Nigerian J. Soil Environ. Res. 7, 82–91.
Teixeira, D.D.B., Marques Jr., J., Siqueira, D.S., Vasconcelos, V., Carvalho, O.A., Martins, É.S., Pereira, G.T., 2018. Mapping units based on spatial uncertainty of magnetic susceptibility and clay content. Catena 164, 79–87. https://doi.org/10.1016/j.catena.2017.12.038.
Thornthwaite, C.W., 1948. An approach towards a rational classification of climate. Geograph. Rev London.
Torrent, J., Barrón, V., 2002. Diffuse reflectance spectroscopy of iron oxides. Encycl. Surf. Colloid Sci. 1438–1446.
Torrent, J., 2005. Mediterranean soils. In: Hillel, D. (Ed.), Encyclopedia of Soils in the Environment. Academic Press, London, pp. 418–427.
Torrent, J., Barrón, V., 2008. Diffuse Reflectance Spectroscopy. In: Ulery, A.L., Drees, L.R. (Eds.), Methods of Soil Analysis – Part 5. Mineralogical Methods. Soil Science Society of America Journal, Madison, pp. 367–385.
Troeh, F.R., 1965. Landform equations fitted to contour maps. Soil Sci. Soc. Am. J. 263, 616–627. https://doi.org/10.2475/ajs.263.7.616.
Vasconcelos, V., Carvalho Júnior, O.A., Martins, E.S., Couto Júnior, A.F., Guimaraes, R.F., Gomes, R.A.T., 2012. Sistema de classificação geomorfométrica baseada em uma arquitetura sequencial em duas etapas: árvore de decisão e classificador espectral, no Parque Nacional da Serra da Canastra. Rev. Bras. Geomorfologia 13, 171–186.
Vieira, S.R., 2000. Geoestatística em estudos de variabilidade espacial do solo. In: Novais, R.F., Alvarez, V.H., Schaefer, G.R. (Eds.), Tópicos em ciência do solo. Sociedade Brasileira de Ciência do Solo, Viçosa, pp. 1–54.
Viscarra Rossel, R.A., Bui, E.N., Caritat, P., McKenzie, N.J., 2010. Mapping iron oxides and the color of Australian soil using visible-near-infrared reflectance spectra. J. Geophys. Res. 115, 1–13. https://doi.org/10.1029/2009JF001645.
Viscarra Rossel, R.A., McGlynn, R.N., McBratney, A.B., 2006. Determining the composition of mineral-organic mixes using UV-vis-NIR diffuse reflectance spectroscopy. Geoderma 137, 70–82. https://doi.org/10.1016/j.geoderma.2006.07.004.
Warrick, A.W., Nielsen, D.R., 1980. Spatial variability of soil physical properties in the field. In: Hillel, D. (Ed.), Applications of Soil Physics. Academic Press, New York, pp. 319–344.
Zheng, H., Wu, J., Zhang, S., 2009. Study on the spatial variability of farmland soil nutrient based on the kriging interpolation. In: AICI, International Conference on Artificial Intelligence and Computational Intelligence, Nowember 7–8 Shanghai, China, pp. 550–555.